Applied Acoustics 216 (2024) 109796

Contents lists available at ScienceDirect

Applied Acoustics

journal homepage: www.elsevier.com/locate/apacoust

A robust optimised multi-material 3D inkjet printed elastic metamaterial

Lawrence Singleton [a,*], Jordan Cheer [a], Anil Bastola [b], Christopher Tuck [b], Steve Daley [a]

[a] Institute of Sound and Vibration Research, University of Southampton, University Road, Southampton, SO17 1BJ, Hampshire, UK
[b] Centre for Additive Manufacturing, Faculty of Engineering, University of Nottingham, Jubilee Campus, Nottingham, NG7 2RD, Nottinghamshire, UK

ARTICLE INFO

Keywords:
Vibration
Metamaterial
Optimisation
Metaheuristics
Additive manufacturing

ABSTRACT

This paper presents and validates a novel elastic metamaterial design, that is optimised for broadband robust vibration control of a structure in the presence of uncertainties, and realised using multi-material additive manufacturing. A novel concept resonator design that allows the resonance frequency to be flexibly tuned via both geometrical and material property modifications is presented and characterised. A unit cell consisting of 12 of these resonators is then proposed. The resonance frequencies and damping ratios of this elastic metamaterial unit cell when attached to a parametrically uncertain example structure are then optimised using a Particle Swarm Optimisation to maximise the mean attenuation in kinetic energy of a structure with parametric uncertainties, based on an analytical model of the system. The performance of the optimised metamaterial is then validated experimentally, and it is shown that the realised metamaterial design is able to achieve a mean of 3.5 dB of broadband attenuation in the presence of uncertainties in the structure. In addition, in the presence of structural uncertainties the robustly optimised design achieves 0.5 dB greater mean attenuation than a design optimised on the nominal structural response alone, and reduced variation in attenuation for different levels of uncertainty.

1. Introduction

As the conservation of materials and fuel becomes increasingly important, structural elements are made thinner and lighter. However, this makes them more compliant and more receptive to vibration. This can lead to structural fatigue or acoustic disturbance, the impact of which can be significant. Tuned Vibration Absorbers (TVAs) offer narrowband vibration attenuation when their resonance frequency is tuned to closely coincide with a target frequency [1], and robustness to uncertainty in the target frequency can be improved with multiple TVAs with resonance frequencies distributed around the target frequency, even when the total TVA mass is the same [2]. Various approaches to the optimal tuning of multiple TVAs have been considered [3–5], and robust control of multiple modes is also achievable with active and adaptive methods [6,7]. However, traditional TVAs can be bulky and heavy, and may not be suitable when there are weight or space constraints, or when a concentrated control force puts too much load on a thin and lightweight structural element.

Metamaterials offer a potential solution to these challenges. A metamaterial consists of sub-structures that interact with waves at a sub-wavelength scale to produce unusual effective material properties, such as negative bulk modulus/stiffness or density/mass [8]. Elastic Metamaterials (EMMs) are metamaterials that can interact with elastic waves in solids. Through careful design, EMMs can interact with elastic waves in a number of ways, but the interest here is in their use as structural vibration absorbers [9–12]. A locally resonant metamaterial consists of an array of resonant sub-structures, and following the principles of TVAs, can be designed to absorb vibration from a primary structure, but with the control force distributed over a larger area. This is potentially a more suitable solution for thin and lightweight structures where a control force concentrated on a small area would need to be constrained to prevent structural fatigue or deformation under gravity due to mass loading, and it also potentially leads to a more compact solution.

The mechanism of absorption in locally resonant EMMs was demonstrated in early examples to be related to the motion of the resonators cancelling out the motion of the structure [13,14]. In [9] it was shown that for flexural vibrations, the resonator motion must be translational rather than rotational, to exert a straightening force on the structure. Similar to the work involving TVAs in [2], distributing the tuning frequencies of multiple resonators around a target frequency has been shown to achieve greater attenuation of a target frequency, and robustness to uncertainty in that frequency, when compared to a single tuning frequency, and this can be extended to multiple target frequencies [15,12]. Broadband control of vibration can also be achieved with

* Corresponding author.
E-mail address: l.r.singleton@soton.ac.uk (L. Singleton).

https://doi.org/10.1016/j.apacoust.2023.109796
Received 3 July 2023; Received in revised form 29 November 2023; Accepted 30 November 2023
Available online 8 December 2023

gradient metamaterials, where the dynamics of the repeated substructures, and therefore the effective frequencies, are graded over the area of the metamaterial [16]. However, for true broadband control, the step change in dynamics between adjacent substructures must be small and therefore the number of differently tuned resonators required to achieve a wide operational bandwidth will be large. Disorder (random variation in the dynamics of individual substructures) can also be shown to increase the bandwidth of control as long as the scale of the variation is small [17]. However, disorder can also result in frequency dependent localisation or trapping of elastic waves [18], which could reduce the effect of the metamaterial by saturating some of the resonant substructures and leaving others poorly coupled. For all of these approaches, a complex design procedure results from the need to keep the number of variously tuned resonators within practical limitations without significantly impacting the performance. Multi-variable design problems such as these lend themselves to metaheuristic optimisation algorithms, as very little information about the system is needed to achieve a high performing result. Algorithms such as Genetic Algorithms and Particle Swarm Optimisation have previously been demonstrated as effective methods of designing multiple TVA and elastic metamaterial vibration absorbers [19–21].

The first locally resonant EMM consisted of spherical masses set into the centre of rubber cubes [22], and since then designs have included: cantilever resonators, with [23,24] or without [25] mass loading; mass-loaded helical springs [26]; and pendula [27]. More complicated cut-out geometries based on cantilever motion have also been used [28], and zig-zag cantilevers have been used to significantly lower the resonance frequencies by folding the beam on itself [29], similar to the folded Helmholtz absorbers used in some acoustic metamaterials [30].

Additive Manufacturing (AM) enables rapid prototyping due to its highly digital nature, with the ability to manufacture devices of varying sizes, from micro to macro scales [31]. There are several AM techniques, with some techniques capable of printing multiple materials simultaneously, potentially allowing different parts of an EMM to have different material properties. For example, depending on the available materials, this could allow the selection of damping characteristics, or provide flexibility in the stiffness or mass of different elements of an EMM to enable its response to be tuned. One possible multi-material AM method is Fused Deposition Modelling (FDM), which is a thermoplastic extrusion based method and multi-material printing can be achieved by pausing the print, purging material from the print head and replacing the material, or by using multiple print heads [32]. The primary challenges associated with multi-material FDM printing include achieving accurate alignment and adhesion between different filament materials, controlling filament flow and deposition, as well as the limited print resolution characteristic of FDM. Another possible multi-material AM technique is vat polymerisation, which uses an ultraviolet laser to convert a liquid photo-polymer into a solid 3D object layer-by-layer. The print platform sits above the liquid vat, and moves away from the vat after each layer is formed, to allow the next layer to be cured. Stereolithography involves multiple vats of different photopolymers mounted on a carousel, which rotates to allow material switching [33]. Printing multi-material parts using stereolithography can be challenging, particularly because of material compatibility, cleanliness, cross-contamination, and process complexity [34]. Finally, 3D inkjet printing is another AM process, that is comparable to its 2D counterpart, and therefore, through the use of multiple ink cartridges is capable of printing continuously between different materials [35]. Inkjet 3D printing is a versatile method that can print a variety of materials including elastomers, rigid polymers, and functional materials, such as conductive and biological materials. With high resolution and the ability to simultaneously print multiple inks, it is also possible to create multi-material and multiple parts on the same print bed. This makes it ideal for producing small-scale resonator arrays with varying materials and geometries. Additionally, the facile scalable nature of ink jetting methods offers the possibility of developing large-scale resonators in the future. Geometric tolerances of AM methods for polymers can vary [36,37], and although the geometric uncertainty of 3D inkjet printing has not been investigated in the literature, Stratasys specify a highest tolerance of around ±0.06% of the dimensions of the object, down to a minimum of ±100 μm for objects less than 100 mm in length [38]. The material properties of 3D inkjet printed parts are also dependent on layer thickness and orientation [39], and on scale [40]. Uncertainties in the geometry and material properties have the potential to cause disorder in the metamaterial, which as already discussed, could impact the performance.

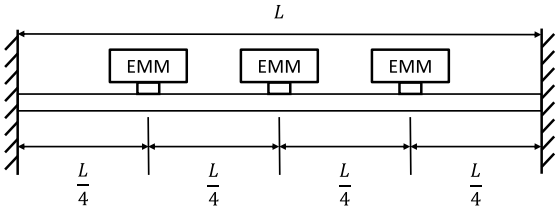

Fig. 1. A diagram of the fixed-fixed beam structure used for evaluation of the optimisation procedure and EMM performance, showing the orientation and location of the EMM unit cells.

This paper proposes and validates a novel, optimised EMM design for robust vibration control of a structure subject to a uniform broadband force excitation. The EMM is realised using multi-material additive manufacturing enabling the dynamics of the EMM to be flexibly tuned. The EMM is based on a resonator design previously presented by the authors in [41] and utilises the robust optimisation approach set out in [21], which provides a design procedure for the robust absorption of multiple modes of flexural structural vibration in the presence of structural uncertainties. First, the potential for AM of the proposed EMM using 3D inkjet printing is investigated, with a focus on the potential to quickly realise multi-material resonators with predictable dynamics. This is achieved by characterising the dynamics of the resonator design for different combinations of geometry and material. The resonance frequencies and damping ratios of the resonators forming the EMM design are optimised using a Particle Swarm Optimisation (PSO) algorithm, and the results are experimentally validated. The following sections first set out an example host structure. A concept resonator design is then proposed, before characterising the effect of suspension geometry and material on the dynamics. Next, the procedure and results of an optimisation study used to select the responses of a multi-resonator EMM unit cell are set out, and finally, the optimised EMM is validated experimentally before conclusions are drawn.

2. Example host structure

In order to investigate the design of the proposed EMM for the robust absorption of vibration, an example structure is considered. The EMM is attached to this structure, and the dynamic response of the structure with and without the EMM attached is used to quantify the performance and design approach.

A beam that fits classical beam theory is useful as an example structure because of the relative simplicity of the respective one dimensional analytical model, and the ability to realise such a structure with relative ease for experimental validation; this study thus utilises a fixed-fixed beam. The EMM unit cell is defined as a group of one or more resonators, that is repeated over the structure. The number of EMM unit cells that are attached to the structure in this study is kept to a total of three, to limit the amount of time taken to fully validate the manufactured EMM unit cells. Fig. 1 shows a diagram of the fixed-fixed beam, with the mounting points of three EDMM unit cells shown.

To demonstrate the performance of the proposed EMM, a lightweight beam that is large enough to attach and support the EMM is formed by two parallel aluminium box sections of external size 20 mm (w) × 10 mm (h) and a wall thickness of 2 mm. The two beams are glued together along the short side and excited by a shaker with a “stinger”

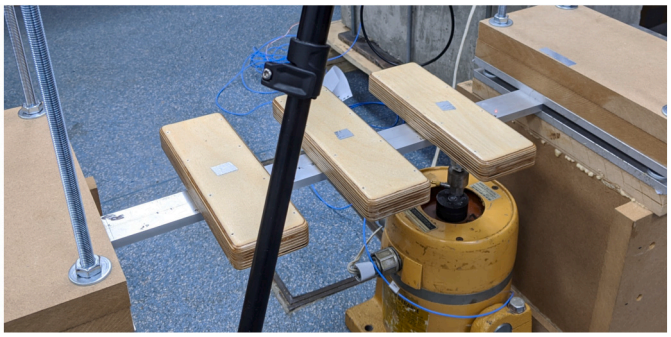

Fig. 2. The practical structure used for the evaluation of the EMM design procedure.

attachment as close to the boundary as the dimensions allow, which is 8 cm. Each end of the beam is clamped to the top of an inert box. The length of the beam can be modified by adjusting the clamping points and this allows uncertainty to be introduced into the structure to evaluate the robust performance of the proposed EMM, which will be discussed further in Section 4.3. To attach each of the EMM unit cells consisting of multiple resonators to a point on the beam, lightweight and stiff platforms made from 18 mm structural plywood have been used, with a small strip of aluminium attached to the underside to minimise the contact patch on the beam and therefore the associated localised additional stiffness and damping. A strip of double sided, high-bond adhesive tape is used to secure the plywood platform to the beam structure. Fig. 2 shows a photo of the structure without the EMM in place.

3. Concept resonator design

In order to realise a locally resonant EMM, a resonant substructure must be designed. In this paper, it is proposed that an array of resonators will be used to control flexural vibration. As demonstrated in [9], it is the translational motion of the oscillating mass that opposes and cancels out the acceleration of the structure. A translational resonator is therefore proposed, with a design that aims to constrain its response to a single degree of freedom to avoid amplifying vibration through out-of-plane resonances. This section sets out the design geometry of a concept resonator, and the proposed changes that will be used to tune its dynamic response. The effect of changes in the geometry and materials are then characterised experimentally, and these results are used as the basis for an EMM optimisation study that is presented in the following section.

3.1. Design geometry

There are several possible approaches to resonator design, including mass-on-beam designs [42] or masses embedded in elastomers [22]. However, achieving low resonance frequencies with these approaches would require a very long beam or a large mass, neither of which are suitable for the compact and lightweight applications that are relevant to the metamaterials considered here. Wire helical springs can have very low stiffnesses, but a single spring does not constrain the motion of an attached mass to a single plane. Designs which incorporate cut-outs from the host structure are also not suitable if the metamaterial is to be fixed to an existing structure or there is a chance of requiring replacement at a later date to account for a change in structural modes or damage. Therefore, a suspension combining the benefits of both a cantilever beam and a helical coil is proposed here. The zigzag beams discussed in [29] obtain a high effective length, and therefore low resonance frequency, in a small form factor, by folding the beam back on itself. However, zigzag beams have complex responses as they are essentially formed from a number of individual cantilever beams coupled

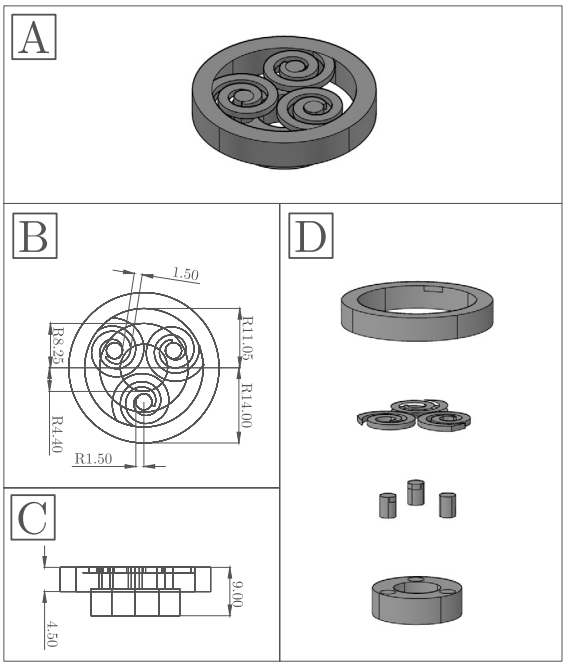

Fig. 3. Diagrams of proposed resonator design. A: Isometric. B: Parallel top. C: Parallel front. D: Exploded view.

by tip accelerations, and standing waves form in the individual sections [43]. Alternatively, coiling a beam into a flat spiral means that a long effective length can be achieved, but as there are no sudden changes in impedance, the response along the length will be much closer to that of a straight beam. Constraining the motion of a mass suspended by coiled beams requires multiple points of contact. A mass suspended on a single flat spiral beam will be unbalanced and experience significant rocking motion. It is therefore proposed to suspend a mass from three flat spiral beam springs. The dimensions of the mass must be such that rotational moments are small compared to the force generated by the acceleration of the mass in its intended direction. Fig. 3 shows a detailed drawing of the proposed resonator geometry, in A: as a 3D solid; B: an aerial view of a line drawing with the dimensions shown for the structural control application set out in Section 2; C: a side view of a line drawing with the dimensions shown for the same application; D: a 3D exploded view showing how the individual elements come together as a whole. This design uses a ring mass, as this allows the mass to be large without needing to be tall, and allows it to be suspended from three flat spiral beams as discussed. The three spiral beams are contained within the ring mass, spaced equidistant around the inner circumference. Each spiral beam is fixed by its centre to the top of a supporting cylindrical column, and these columns are mounted to a ring shaped base, which fits inside the ring mass and can be fixed to the host structure. This design means that the ring mass is free to oscillate without being impeded by any other elements.

3.2. Modifying the dynamic response

The resonance frequency of the proposed resonator design could be changed via a number of mechanisms. Initially, considering changes in the geometry of the resonator design, it is possible to tune the resonance frequency via various modificiations. Firstly, scaling the entire resonator would change its resonance frequency, but for an array of differently tuned resonators, keeping the footprint constant is advantageous as the array can be laid out in a uniform arrangement with the smallest practical spacing. Therefore, tuning the resonance frequency by changing the mass of the ring through an increase in its volume is also limited. Reducing the inner circumference of the ring mass to in-

Fig. 4. Resonator with suspension made from a material that is too flexible to be suitable, causing the mass to sag significantly under gravity (left), compared to a resonator made completely from VeroClear (right).

crease its volume would maintain a constant footprint, but would also mean reducing the maximum possible size of the suspension, which would reduce its effective length, increasing its stiffness and negating some or all of the effect of the mass increase. Increasing the height of the mass without increasing the volumetric footprint of the resonator means reducing the distance between the ring mass and the host structure, which will limit the maximum displacement. The thickness and number of turns in the suspension coils is a simple geometrical change that does not modify the footprint of the resonator. The flexural stiffness of a beam is directly related to the cube of its thickness and the length, so the relationship to the resonance frequency will provide a curve that can be used to map a geometry to a required tuning frequency.

As noted in the introduction, the resonator will be manufactured using 3D inkjet printing. Therefore, depending on the capabilities of the inkjet system, it may also be possible to tune the resonance frequency through changes to the material composition of the resonator design. The system that has been used in this study is a Stratasys Objet260 Connex, which facilitates the mixing of different materials in different proportions to create "Digital Materials". This study considers mixes between two different primary materials: VeroClear (RGD810), a clear, acrylic-like polymer (Shore hardness D 83-86); and Tango Black (FLX973), a black, and highly flexible elastomer (Shore Hardness A 26-28). Initial experimentation highlighted that VeroClear and three of the digital mixes are suitable for use in these resonators: RGD8710, RGD8720 and RGD8730 are the first three mixes with increasing proportions of Tango Black added, and therefore decreasing stiffness. More flexible materials are possible, but the displacement of the ring mass under gravity becomes significant (as shown in Fig. 4). These materials are all of the same density, and they therefore cannot be used to change the mass of the moving ring mass. As the coiled beam suspension is the only element of the discussed resonator design that is designed to be flexible, it is proposed that this element can be made from a different material, but the mass, base and supporting columns of the resonator will be made solely from VeroClear. Selecting materials with different stiffnesses for the suspension coils provides another method of changing the resonance frequency. Samples of Tango Black are also visibly highly viscoelastic (loss factor > 0.1), and it is expected that as the proportion of this material in the mix increases, so will viscous losses. This means that the suspension material can also be chosen to change the damping ratio of the resonator.

3.3. Validation of resonator dynamics

To begin to validate the performance of the proposed novel resonator design, a resonator made solely of VeroClear with a suspension coil thickness of 1 mm has been printed, with four copies produced to assess variability. The printing process means that the resonators are encased in a soft, flexible support material, which was removed by hand with mechanical tools. In order to measure the frequency response for comparison to the simulations, the resonator was fixed to the top of a large electrodynamic shaker along with an accelerometer, as shown in Fig. 5. The shaker was driven with broadband white noise and the velocity of the moving ring mass was then measured using a laser vibrometer focussed at the junctions between the ring mass and each coiled suspension element. The sampling frequency was set to 4 kHz, and all signals were passed through a KEMO low-pass filter with a cut-off frequency of 1.5 kHz to provide anti-aliasing.

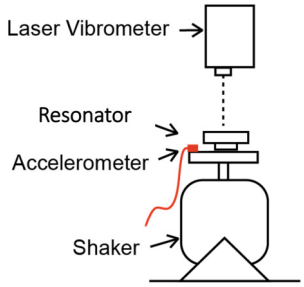

Fig. 5. Experimental setup for the measurement of the printed resonator dynamic responses.

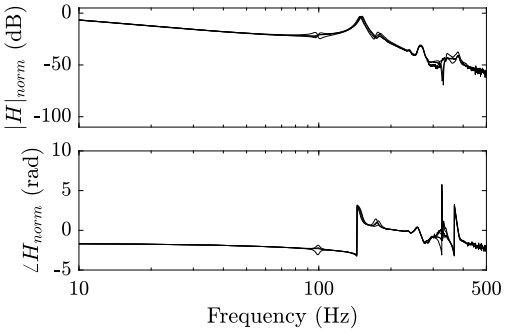

Fig. 6. Magnitude (top) and phase (bottom) of the max-normalised frequency response between the acceleration of the base and the velocity of the mass for all four prints of the resonator made from VeroClear with a 1 mm thick suspension.

Fig. 6 shows the magnitude and phase of the max-normalised transfer function, H_{norm}, calculated between the acceleration of the base and the velocity of the mass ring for all four resonators at a single point. From Fig. 6 it can be seen that the responses of each print are very similar, and that the resonance frequencies of the printed resonators are in the range 148–152 Hz. By observing the difference in the velocity magnitude and phase response of the ring mass at the different measurements positions, the frequency response above 200 Hz was seen to consist of low amplitude out-of-plane and rocking modes, most likely introduced by non-ideal base excitation.

3.4. Experimental characterisation of multi-material resonators

The proposed resonator design was printed with coil suspension thicknesses of between 0.6 and 3.0 mm, in increments of 0.2 mm. Four resonators of each thickness were printed, and the resonance frequency of each resonator was measured using the same procedure as set out in Section 3.3. Fig. 7.a shows the resonance frequency, f_r and Fig. 7.b the damping ratio, ζ, estimated using the logarithmic decrement of the impulse response of the transfer function, for resonators with coil suspension thicknesses between 0.6 and 3 mm, and with the coil suspension made from each of the four practical materials discussed in Section 3.2. From Fig. 7.a it can be seen that although the more flexible mixes, RGD8710 (— —) and RGD8720 (— - — -), do achieve a slightly lower resonance frequency than VeroClear (—), RGD8730 (· · ·) reduces it by a significant amount. From Fig. 7.b it can be seen that the estimated damping ratio is fairly consistent across thicknesses for each of the materials. Table 1 shows the mean damping ratio, $\hat{\zeta}$, estimated for the resonators made with each of the four materials, and shows that each material offers a different mean damping ratio, such that this multi-material printing approach allows both the resonance frequency

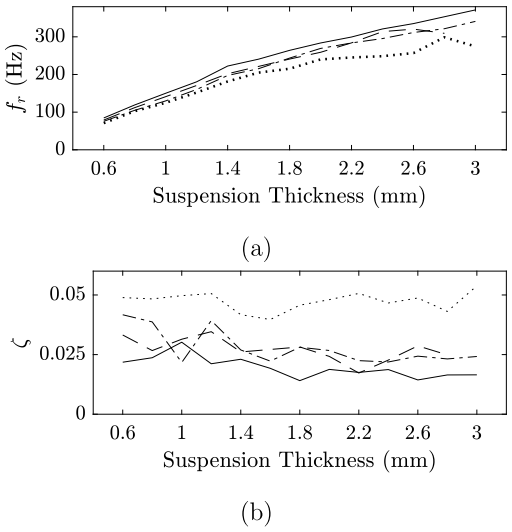

Fig. 7. a) measured resonance frequency, f_r, for the resonator design with different coil suspension thickness with the suspension made from: VeroClear (—); RGD8710 (— —); RGD8720 (— - — -); RGD8730 (· · ·). b) estimated damping ratio, ζ, for the resonator design with different suspension thickness with the coil suspension made from: VeroClear (—); RGD8710 (— —); RGD8720 (— - — -); RGD8730 (· · ·).

Table 1
Mean damping ratio, $\hat{\zeta}$, of the resonators manufactured with the suspension made from each of the different materials.

Material	$\hat{\zeta}$
VeroClear	0.020
RGD8710	0.024
RGD8720	0.028
RGD8730	0.047

and damping of the printed resonator to be tuned, offering additional design freedom. This makes the proposed resonator design, and the proposed multi-material manufacturing approach, highly practical from a design point of view, as the damping ratio can be selected by choosing one of the available materials, and then the thickness required to achieve a certain resonance frequency easily calculated by mapping it to the curves presented in Fig. 7.a.

4. Optimisation of an EMM unit cell

The previous section has set out the concept design of a SDOF resonator, printed using multi-material 3D inkjet printing from a combination of rigid and flexible polymer-based materials. It is next proposed that this resonator, grouped into unit cells of multiple resonators and repeated over the structure, can be tuned in terms of resonance frequency and damping to perform as an elastic metamaterial for the absorption of vibration. This section sets out a design process for a multi-resonator unit cell using these resonators applied to an example host structure. The design method utilises a Particle Swarm Optimisation to determine the optimal resonance frequencies and damping ratios for each resonator, based on the robust optimisation approach set out in [21]. As in the previous study, it is assumed that the structure will be subject to an unknown disturbance, and therefore the response across frequency must be considered with equal importance, and this is achieved by utilising a uniform broadband force as the disturbance during the optimisation. Subsequently, the optimisation results will be used in combination with the results from the experimental characterisation of the resonators set out in the previous section to select the required suspension geometries and materials.

4.1. EMM design

A unit cell of 12 independently tuned resonators has previously been shown to achieve a reasonable level of robust control of three structural modes [20]. This provides a compromise between achieving robustness with a wide and dense distribution of tuning frequencies, and limiting the number of resonators so that the design process is simplified and the unit cell is small in size compared to the wavelengths involved. The unit cell resonators are arranged in a 6×2 grid with the bases interconnected by thin bars to improve the ease of mounting, as shown in Fig. 8.

The concept resonator design with 2 turns in the suspension coils has been shown to achieve resonance frequencies spanning the range of approximately 80–350 Hz. It is possible to achieve higher resonance frequencies by reducing the number of turns in the coils of the suspension, and a similar experiment to that carried out in Section 3.4 has been carried out to characterise a resonator with 1.5 turns in the coil suspension. The full characterisation of the resonators indicates that the resonance frequency of the considered resonators can be tuned anywhere in the range of 80–500 Hz. To match this tuning capability, the considered uncertain host structures described in Section 2 have been specified to have the first three modal resonance frequencies between 80 and 500 Hz.

4.2. Optimisation strategy

An analytical modal model where attached resonators are expressed as additional impedances, has been used to simulate the velocity frequency response, and total structural kinetic energy of the structure, with and without the EMM attached in order to evaluate the performance. The resonance frequency and damping ratio of each resonator in the unit cell is optimised consecutively using a PSO, with each result carrying forward until a result has been found for all 12. This sequential approach was shown in initial experimentation to achieve a better performance than optimising all resonators simultaneously with very little increase in computation time, despite requiring the algorithm to be run twelve times, due to the much simpler cost surface. Although the resonance frequency and damping ratio are the design parameters that are directly optimised, these must be translated into the required coil suspension geometry and material based on the resonator characterisation presented in Section 3. This means that the resonance frequency in the optimisation must be constrained to the range that can be obtained within the limitations of the resonator design; the resonance frequencies in the optimisation are thus constrained to be between 80 and 500 Hz. The damping ratio must be constrained to the four possible damping ratios provided by the four available materials. In order to impose this optimisation constraint, a dimensionless non-integer variable is optimised and used to index to the four possible materials and damping ratios. This variable is bounded between 0.5 and 4.5, and the output value is then rounded to the nearest integer to give an integer from 1 to 4 which indexes to the damping ratio of VeroClear, RGD8710, RGD8720 and RGD8730 respectively.

The PSO was implemented using the particleswarm function in MATLAB, running in parallel on a high performance computing cluster. The optimisation was initially run for a nominal structure, to provide comparison to a robust optimisation that takes into account uncertainties in the structural response, which was shown in [20] to result in a significant improvement in the vibration control of an uncertain structure. The nominal structure has a length of 49 cm, which achieves three modes centred within the defined frequency range. The objective in this nominal case is to maximise the attenuation in the kinetic energy of the nominal structure provided by the EMM. The robust optimisation aims to maximise the mean attenuation in kinetic energy of the nominal structure and 59 structures subject to uncertainty in the beam

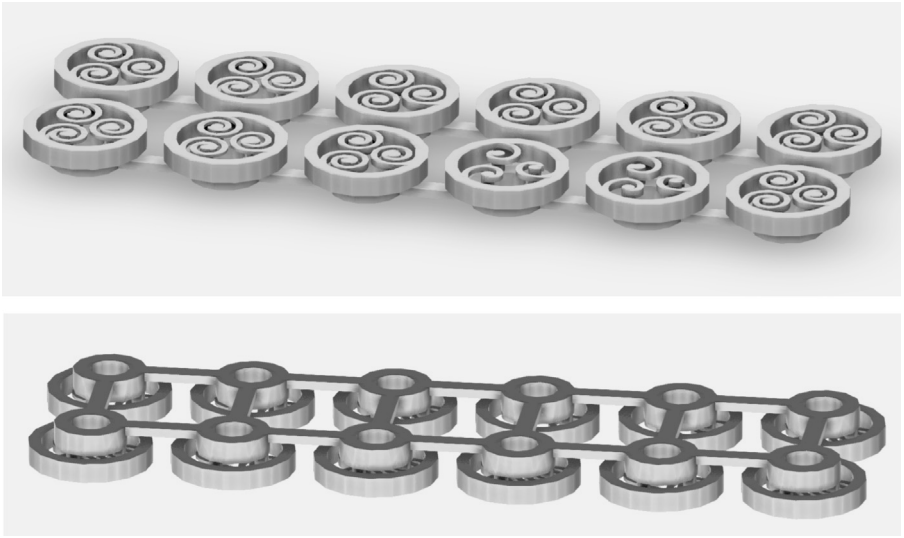

Fig. 8. The proposed EMM unit cell consisting of a 6×2 array of resonators connected by thin bars.

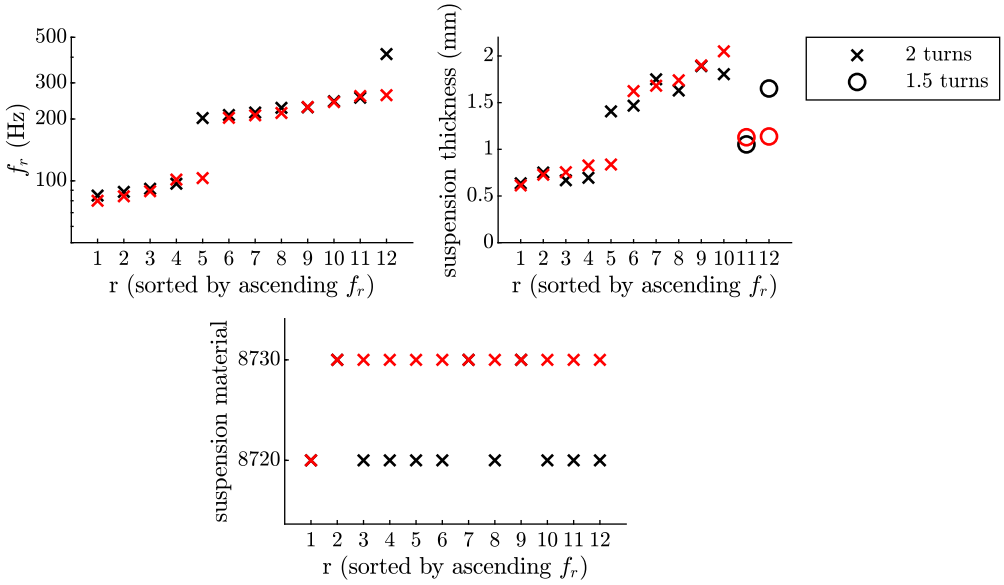

Fig. 9. Optimised resonance frequency (top-left), suspension thickness (top-right), and suspension material (bottom), optimised for: black—the attenuation in the kinetic energy of a nominal structure; red—the mean attenuation in the kinetic energy of an uncertain structure, sorted by ascending resonance frequency.

length. The uncertainty in the length has been restricted to a uniform distribution between 46 cm and 52 cm, resulting in a range of modal frequencies within ±9% of the nominal. The distribution of the EMM unit cells on the structure is relative to the length, therefore retaining the same coupling to the mode shapes. This is a simple way to achieve a change in modal frequencies that can be represented experimentally, but as long as it can be represented analytically the optimisation approach can be modified to take into account other uncertainties in materials properties, mass loading or even non-uniform properties and changes to boundary conditions. As discussed in the literature, 3D inkjet printing introduces geometric uncertainty in the realised metamaterial. However, because the resonators are damped and a distribution in the resonance frequencies is introduced by design, it is considered that uncertainty in the structure will likely have a greater impact on the response in the considered case. Covering all forms of uncertainty within this single study is not feasible, but the considered form of uncertainty gives a methodology for designing in the context of uncertainty in general. The introduction of other forms of uncertainty in the structure, and the manufacturing uncertainties, is relevant future work.

4.3. Optimisation results

Fig. 9 shows the optimised resonance frequency (top-left), suspension thickness (top-right), and coil suspension material (bottom) for the unit cell optimised for a nominal structure only (black) and for robust performance (red), sorted by ascending resonance frequency. From Fig. 9 it can be seen that the optimal resonance frequencies for the nominal condition are mainly grouped into two clusters around 85–97 Hz, and 202–254 Hz, with one resonator tuned to the higher frequency of 415 Hz. The nominal structure has modes at 93 Hz, 231 Hz, and 420 Hz, so it is clear that the optimisation results are consistent with what would be expected from the theory of multiple TVAs set out in the literature, and distributed the tuning frequencies around each mode. The EMM optimised for nominal performance has the majority (9) of the resonators manufactured with the suspension made from the material mix RGD8720, which gives a damping ratio of 0.028. The remaining 3 are manufactured from RGD8730, which gives a damping ratio of 0.047. This indicates that the optimisation process does not maximise damping, but is able to tune the EMM to utilise the resonant absorption

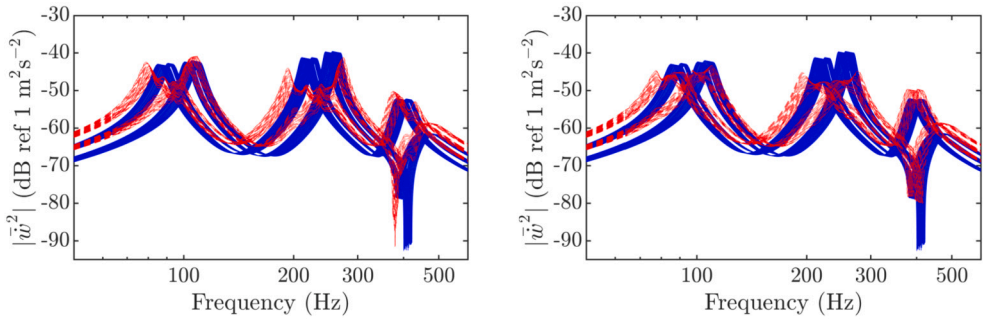

Fig. 10. Mean squared velocity magnitude over time and space, $|\bar{\dot{w}}^2|$, for the structure only (blue) and the structure with the EMM attached (red) for the EMM optimised for nominal performance (left) and for robust performance (right).

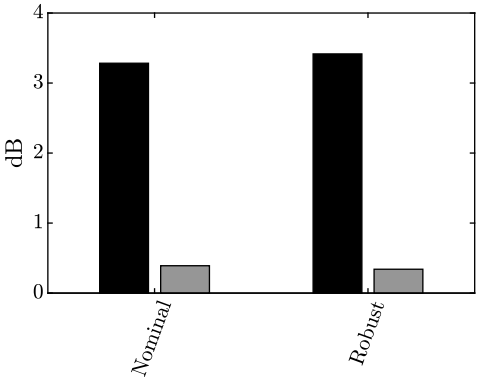

Fig. 11. Simulated mean attenuation in the kinetic energy (black) and the standard deviation of kinetic energy (grey) across uncertain structures.

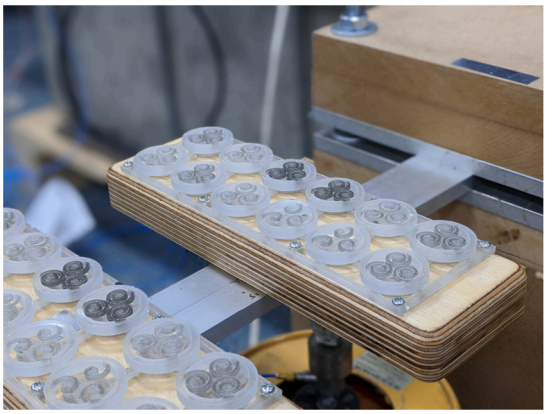

Fig. 12. Printed EMM unit cell glued to a plywood block for experimental validation.

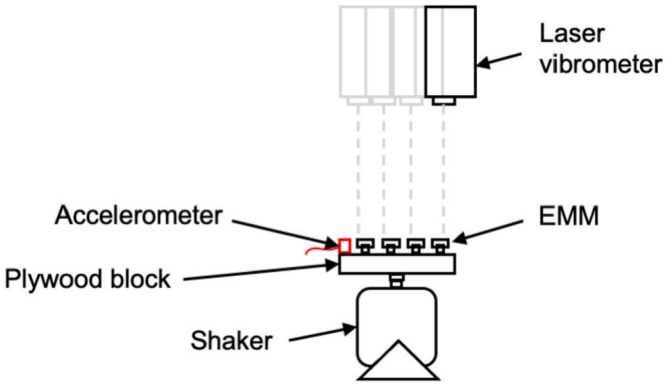

Fig. 13. Experimental setup for measuring the resonance frequency of each member of the EMM unit cell.

effectively. It can be seen from Fig. 9 that the optimal resonance frequencies achieved by the robust optimisation are in two groups, centred around 90 Hz and 230 Hz, with ranges of 80–103 Hz and 203–261 Hz. These ranges are much wider than those for the system optimised based on the nominal structure, which is consistent with what is expected for an uncertain structure. The beam structures with lengths ranging from 46 cm to 52 cm produce the first two modes with frequency ranges 85–111 Hz and 210–269 Hz, and in both cases the EMM frequencies cover the lower bound but not the upper bound. It is probable that the reason for this is that the additional mass from the EMM added to the structure is expected to lower the resonance frequencies slightly, bringing the tuning frequency and modal frequency ranges into alignment. The robust EMM does not tune any of the resonance frequencies to the third mode; this will be discussed below in relation to the velocity frequency responses.

Fig. 10 shows the frequency response of the mean squared velocity, averaged over the length of the structure, $\bar{\dot{w}}^2$, for the structure only (blue) and the structure with the EMM attached (red) for the EMM optimised for nominal performance (left) and for robust performance (right). The plots show both the magnitude (top) and phase (bottom). From these results it can be seen that the robust optimisation achieves greater and more consistent attenuation of the first and second modes in the presence of significant uncertainty, causing a large shift in the modal frequencies, as expected. However, when uncertainty is small, meaning the modal frequencies are still close to the nominal, the EMM optimised for nominal performance achieves greater control. This is probably due to the nominally optimised EMM still utilising resonators with resonance frequencies distributed around the peak in the structural response, and relatively high damping. The third mode is largely unaffected, which is consistent with the lack of resonators tuned around this peak. The third mode is significantly lower in energy and this explains why neither optimisation process tunes resonators around this peak.

To provide a clearer comparison of the two optimisation processes, Fig. 11 shows the simulated robust performance of both the nominally optimised and robust optimised EMM in terms of the mean attenuation in the kinetic energy (black), and the standard deviation in the kinetic energy of the structure (grey). From Fig. 11 it can be seen that the robust optimised EMM achieves only a marginally greater mean attenuation in kinetic energy in this case, as well as reduced variation in the performance between different uncertain structures, as indicated by the lower standard deviation. While still an improvement, this does not appear to be a significant difference and from this information alone it could be interpreted that the robust optimisation is not worthwhile given the increased computational load required to model multiple uncertain cases in each calculation of the fitness function. However, the structural velocities shown in Fig. 10 clearly show an improvement in robustness, particularly in the control of the first structural mode,

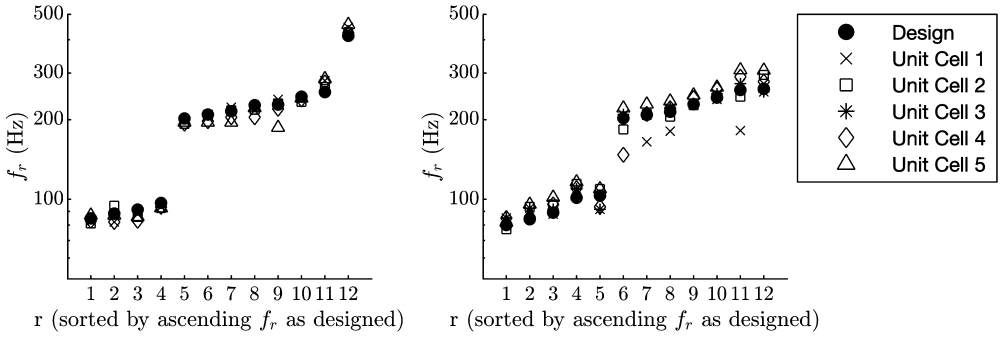

Fig. 14. Resonance frequencies estimated from the velocity frequency response of the resonator masses for nominal (left) and robust (right) unit cells, compared to the design frequencies (shown by solid circles).

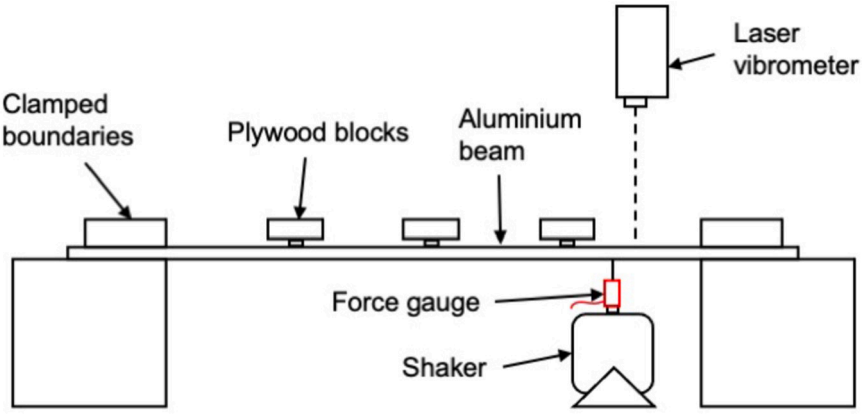

Fig. 15. Diagram of the experimental setup for the validation of the performance of the optimised EMM.

when the uncertainty causes a large shift in the modal frequency. Therefore, although the difference in the mean attenuation in kinetic energy (the robust fitness function) is small, the robust optimisation has still achieved a desirable improvement in robustness to structural uncertainties.

5. Experimental validation

The results of the optimisations set out in the previous section give a set of coil suspension geometries and materials that are used to realise the EMM unit cell design. Both nominal and robust optimised unit cells have been printed using 3D inkjet printing, with five of each design being printed in order to be able to assess variability in their responses. In this section, the experimental procedure is first described, before the resonance frequencies of each resonator in each of the unit cells are measured and compared to their expected values. The performance of the nominal and robust optimised EMM unit cells is then evaluated when they are attached to a practical structure that is consistent with the structure outlined in Section 2.

5.1. Unit cell dynamics

The EMM unit cells were glued to plywood blocks, as shown in Fig. 12, matching those forming part of the structure, previously described in Section 2. In order to compare the expected resonance frequencies with those actually achieved, the experimental method described in Section 3.3 has been repeated, but instead of fixing a resonator to the top of the shaker, each EMM unit cell block was fixed to the shaker, and the laser vibrometer moved to measure the velocity of each resonator mass individually, as shown in Fig. 13.

Fig. 14 shows the estimated resonance frequencies of all five printed unit cells for the nominal (left) and robust (right) designs, evaluated by taking the frequency of the highest peak in the velocity frequency response. From Fig. 14 it is shown that there is in general a reasonable agreement between the measured and the designed resonance frequencies. There are a few anomalous results, which are due to a splitting of the resonance. This could be caused by interaction with rocking modes, or possibly plastic deformation during the support material removal process. Carried forward to the experimental validation are the nominal unit cells numbered 2, 3 and 4, and the robust unit cells numbered 2, 3 and 5, as this avoids the unit cells with anomalous results.

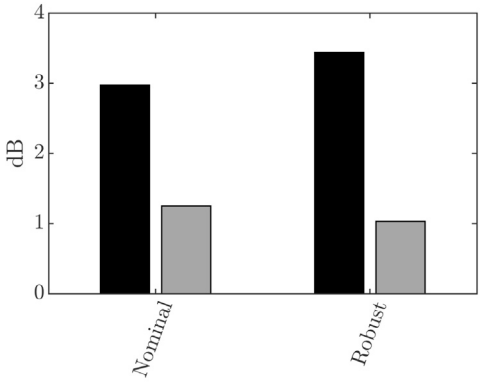

Fig. 16. Measured mean attenuation in the kinetic energy estimate (black) and standard deviation (grey) of the kinetic energy estimate across uncertain structures.

5.2. EMM performance

The performance of the EMM unit cells has been evaluated by measuring the dynamic response of the host structure described in Section 2,

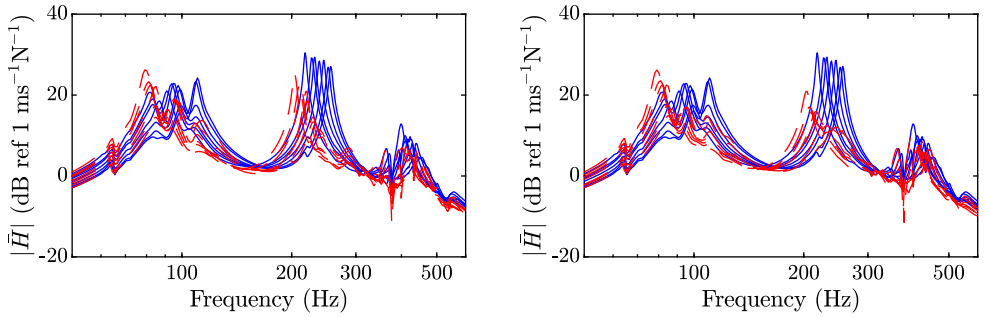

Fig. 17. Spatially averaged mobility FRF magnitude of the uncontrolled structure (blue—solid) and the structure with the optimised EMM attached (red—dashed) for: Left — the EMM optimised based on the nominal modelled structure only; Right — the EMM optimised based on the uncertain modelled structures.

with and without the EMM attached when the structure is excited by a shaker driven with white noise. The host structure was measured at 7 equally spaced points along the length of the beam using a laser vibrometer, and the excitation force was measured using a force gauge. Fig. 15 shows a diagram of the measurement setup.

The beam velocity was measured without the EMM, with three nominal EMM unit cells, and with three robust EMM unit cells, for beam lengths of 46–52 cm in 1 cm increments (a total of 7 discrete lengths), which is consistent with the variations in the beam response assumed in the simulations used to optimise the EMM designs. Fig. 16 shows the mean and standard deviation of the attenuation in the estimated kinetic energy (calculated from the mean squared velocity measured at 7 discrete locations along the beam) achieved for each of these beams for the nominal and robust optimised EMMs. From Fig. 16 it can be seen that the robust optimised EMM achieves a greater mean attenuation and a lower standard deviation than the design based on the nominal response alone. This is inline with the simulated results produced by the optimisation study. The mean attenuation for the EMM optimised for the robust response is very similar to the simulated value, however, the value for the EMM optimised based on the nominal response only is marginally lower. A small difference is to be expected due to the differences between the model and the realised system. The standard deviation is significantly higher in the measured results compared to the simulations.

To help provide further insight into the statistical results presented in Fig. 16, Fig. 17 shows the measured spatially averaged mobility FRF, $\bar{H}$, for the nominal (left) and robust (right) optimised EMM (red-dashed) compared to the structural velocity with no EMM (blue-solid) for all 7 beam lengths. From these results it can be seen that there is some robust attenuation in the third mode in both cases, despite the lack of resonators tuned to this frequency region and this differs from the attenuation performance seen in the simulations. Significant attenuation is also seen in the second mode, with a clear improvement in attenuation when the mode is shifted lower in frequency for the robust optimised EMM. However, both nominal and robust optimised EMMs perform similarly around the first mode, with significant attenuation for some beam lengths but not for others. In some cases, both EMMs generate enhancement in the response of the first mode. It can also be seen that there is a splitting of the first mode in the measured response, probably due to out-of-plane motion such as torsional vibration. This split mode has a wider bandwidth compared to a single mode, and the enhancement occurs at a frequency that is outside of the frequencies that the resonators in both EMM unit cells are tuned to, so they are not able to attenuate the lower frequency resonances of the split mode. The fact that this mode is attenuated for the shortest beam (with the highest frequency) and enhanced for the longest beam (with the lowest frequency) is almost certainly the reason for the large standard deviation value shown in Fig. 16. This issue could be addressed in the EMM design process by increasing the range of structural uncertainty used in the robust optimisation procedure. However, this would result in an overestimation of the uncertainty in the other modal frequencies, where this mode splitting does not occur. To avoid this, the analytical formulation used to simulate the structural dynamics could be weighted such that the response due to the first mode experiences greater uncertainty than the other modes.

6. Conclusions

This paper has presented and investigated the design of a multi-resonator EMM unit cell manufactured using multi-material 3D inkjet printing. The adopted manufacturing process allows complex, high-resolution geometry at a small scale, and the ability to utilise different material properties to control both the resonance frequency and damping of the resonator responses. An experimental study of a novel resonator design has shown that its resonance frequency and damping ratio can be tuned by varying the suspension material and geometry.

In order to evaluate a robust EMM design process, it has been applied to a fixed-fixed beam structure. In the first instance, an EMM unit cell of 12 resonators was optimised using a simulated system for the attenuation of the kinetic energy of a nominal structure only, and also for the mean attenuation of the kinetic energy across a range of structures where the beam is varied in length to achieve a change in the modal frequencies. The results of the simulation-based optimisation demonstrate a clear improvement in robustness when the EMM is optimised for robust performance, as expected. This improvement has been shown to be due to a greater attenuation in the first two modes when the frequencies move away from the nominal response. The third mode, however, was largely unaffected, due to the lack of EMM resonators tuned around this frequency. This is because the third mode has a significantly lower amplitude than the first two modes, so that the optimisation focuses the available resonators around the first two modes.

To validate the EMM and the robust design approach experimentally, the optimised unit cells were printed and the host structure was realised. The resonance frequencies of the printed unit cells were shown to be close to the design frequencies, but with a small degree of variation. Nevertheless, the robust optimised unit cell was shown to achieve greater robust performance than the nominal design, in agreement with the simulation study. There was a significant increase in the standard deviation in the attenuation of the estimated kinetic energy over the range of structures, which has been linked to the enhancement in the first mode in some cases. This enhancement occurs due to an increase in the bandwidth of the first mode, which occurs because of a splitting in the first mode, and the designed unit cells are not sufficiently robust to this.

CRediT authorship contribution statement

Lawrence Singleton: Conceptualisation, Methodology, Investigation, Writing – Original draft preparation. **Jordan Cheer:** Supervision, Writing – Review and editing. **Anil Bastola:** Manufacturing, Investigation. **Christopher Tuck:** Writing – Contributions to manuscript. **Steve Daley:** Supervision.

Declaration of competing interest

The authors declare that they have no known competing financial interests or personal relationships that could have appeared to influence the work reported in this paper.

Data availability

Data will be made available on request.

Acknowledgements

This research was partially supported by an EPRSC iCASE studentship (Voucher number 17100092) and the Intelligent Structures for Low Noise Environments (ISLNE) EPSRC Prosperity Partnership (EP/S03661X/1).

The authors acknowledge the use of the IRIDIS High Performance Computing Facility, and associated support services at the University of Southampton, in the completion of this work.

References

[1] Ormondroyd J, Den Hartog JP. The theory of the dynamic vibration absorber. J Appl Mech 1928;50:9–22.
[2] Igusa T, Xu K. Vibration control using multiple tuned mass dampers. J Sound Vib 1994;175(4):491–503. https://doi.org/10.1006/JSVI.1994.1341.
[3] Li C. Optimum multiple tuned mass dampers for structures under the ground acceleration based on DDMF and ADMF. Earthq Eng Struct Dyn 2002;31(4):897–919. https://doi.org/10.1002/eqe.128.
[4] Li HN, Ni XL. Optimization of non-uniformly distributed multiple tuned mass damper. J Sound Vib 2007;308(1–2):80–97. https://doi.org/10.1016/J.JSV.2007.07.014.
[5] Gardonio P, Turco E. Tuning of vibration absorbers and Helmholtz resonators based on modal density/overlap parameters of distributed mechanical and acoustic systems. J Sound Vib 2019;451:32–70. https://doi.org/10.1016/J.JSV.2019.03.015.
[6] Gardonio P, Zilletti M. Sweeping tuneable vibration absorbers for low-mid frequencies vibration control. J Sound Vib 2015;354:1–12. https://doi.org/10.1016/j.jsv.2015.05.024.
[7] Gardonio P, Turco E, Kras A, Bo LD, Casagrande D. Semi-active vibration control unit tuned to maximise electric power dissipation. J Sound Vib 2021;499:116000. https://doi.org/10.1016/J.JSV.2021.116000.
[8] Dalela S, Balaji PS, Jena DP. A review on application of mechanical metamaterials for vibration control. Mech Adv Mat Struct 2021:1–26. https://doi.org/10.1080/15376494.2021.1892244.
[9] Sun H, Du X, Pai PF. Theory of metamaterial beams for broadband vibration absorption. J Intell Mater Syst Struct 2010;21(11):1085–101. https://doi.org/10.1177/1045389X10375637.
[10] Xiao Y, Wen J, Wen X. Broadband locally resonant beams containing multiple periodic arrays of attached resonators. Phys Lett A 2012;376(16):1384–90. https://doi.org/10.1016/J.PHYSLETA.2012.02.059.
[11] Zhu R, Liu X, Hu G, Sun C, Huang G. A chiral elastic metamaterial beam for broadband vibration suppression. J Sound Vib 2014;333(10):2759–73. https://doi.org/10.1016/J.JSV.2014.01.009.
[12] Peng H, Frank Pai P, Deng H. Acoustic multi-stopband metamaterial plates design for broadband elastic wave absorption and vibration suppression. Int J Mech Sci 2015;103:104–14. https://doi.org/10.1016/J.IJMECSCI.2015.08.024.
[13] Milton GW, Willis JR. On modifications of Newton's second law and linear continuum elastodynamics. Proc R Soc A, Math Phys Eng Sci 2007;463(2079):855–80. https://doi.org/10.1098/rspa.2006.1795.
[14] Yao S, Zhou X, Hu G. Experimental study on negative effective mass in a 1D mass-spring system. New J Phys 2008;10(4):043020. https://doi.org/10.1088/1367-2630/10/4/043020.
[15] Pai PF. Metamaterial-based broadband elastic wave absorber. J Intell Mater Syst Struct 2010;21(5):517–28. https://doi.org/10.1177/1045389X09359436.
[16] Wu X, Wen Z, Jin Y, Rabczuk T, Zhuang X, Djafari-Rouhani B. Broadband Rayleigh wave attenuation by gradient metamaterials. Int J Mech Sci 2021;205:106592. https://doi.org/10.1016/J.IJMECSCI.2021.106592.
[17] Hao S, Wu Z, Li F, Zhang C. Enhancement of the band-gap characteristics in disordered elastic metamaterial multi-span beams: theory and experiment. Mech Res Commun 2021;113:103692. https://doi.org/10.1016/J.MECHRESCOM.2021.103692.
[18] Bouzit D, Pierre C. Localization of vibration in disordered multi-span beams with damping. J Sound Vib 1995;187(4):625–48. https://doi.org/10.1006/JSVI.1995.0549.
[19] Mohebbi M, Shakeri K, Ghanbarpour Y, Majzoub H. Designing optimal multiple tuned mass dampers using genetic algorithms (GAs) for mitigating the seismic response of structures. J Vib Control 2013;19(4):605–25. https://doi.org/10.1177/1077546311434520.
[20] Singleton L, Cheer J, Daley S. Metaheuristic optimisation of an elastic metamaterial for robust vibration control. In: Proceedings of meetings on acoustics, vol. 39. Acoustical Society of America; 2019. p. 045008.
[21] Singleton L, Cheer J, Daley S. A robust optimised shunted electrodynamic metamaterial for multi-mode vibration control. J Sound Vib 2022;527. https://doi.org/10.1016/J.JSV.2022.116861.
[22] Liu Z. Locally resonant sonic materials. Science 2000;289(5485):1734–6. https://doi.org/10.1126/science.289.5485.1734.
[23] Li Y, Baker E, Reissman T, Sun C, Liu WK. Design of mechanical metamaterials for simultaneous vibration isolation and energy harvesting. Appl Phys Lett 2017;111(25):251903. https://doi.org/10.1063/1.5008674.
[24] de Melo Filho NG, Claeys C, Deckers E, Desmet W. Metamaterial foam core sandwich panel designed to attenuate the mass-spring-mass resonance sound transmission loss dip. Mech Syst Signal Process 2020;139:106624. https://doi.org/10.1016/j.ymssp.2020.106624.
[25] Wu YT, Hu HL, Lee CY. Finite element analysis of an acoustic metamaterial plate incorporating tunable shape memory cantilever absorbers. J Phys Conf Ser 2020;1509:12002. https://doi.org/10.1088/1742-6596/1509/1/012002.
[26] Lee C-Y, Pai C-A. Design and implementation of tunable multi-degree-of-freedom vibration absorber made of hybrid shape memory helical springs. J Intell Mater Syst Struct 2016;27(8):1047–60. https://doi.org/10.1177/1045389X15581519.
[27] Yoon JY, Song WK, Park N-C. Pendulum-type elastic metamaterial for reducing the vibration of a space tether. Acta Astronaut 2019. https://doi.org/10.1016/J.ACTAASTRO.2019.06.008.
[28] Gao P, Climente A, Sánchez-Dehesa J, Wu L. Single-phase metamaterial plates for broadband vibration suppression at low frequencies. J Sound Vib 2019;444:108–26. https://doi.org/10.1016/J.JSV.2018.12.022.
[29] Abdeljaber O, Avci O, Kiranyaz S, Inman DJ. Optimization of linear zigzag insert metastructures for low-frequency vibration attenuation using genetic algorithms. Mech Syst Signal Process 2017;84:625–41. https://doi.org/10.1016/J.YMSSP.2016.07.011.
[30] Liang Z, Li J. Extreme acoustic metamaterial by coiling up space. Phys Rev Lett 2012;108(11):114301. https://doi.org/10.1103/PHYSREVLETT.108.114301/FIGURES/5/MEDIUM.
[31] Berman B. 3-D printing: the new industrial revolution. Bus Horiz 2012;55(2):155–62. https://doi.org/10.1016/J.BUSHOR.2011.11.003.
[32] Espalin D, Ramirez JA, Medina F, Wicker R. Multi-material, multi-technology FDM: exploring build process variations. Rapid Prototyping J 2014;20(3):236–44. https://doi.org/10.1108/RPJ-12-2012-0112/FULL/PDF.
[33] Choi JW, Kim HC, Wicker R. Multi-material stereolithography. J Mater Process Technol 2011;211(3):318–28. https://doi.org/10.1016/J.JMATPROTEC.2010.10.003.
[34] Shaukat U, Rossegger E, Schlögl S. A review of multi-material 3D printing of functional materials via vat photopolymerization. Polymers 2022;14(12):2449. https://doi.org/10.3390/POLYM14122449.
[35] García-Collado A, Blanco JM, Gupta MK, Dorado-Vicente R. Advances in polymers based multi-material additive-manufacturing techniques: state-of-art review on properties and applications. Addit Manuf 2022;50:102577. https://doi.org/10.1016/J.ADDMA.2021.102577.
[36] Minetola P, Calignano F, Galati M. Comparing geometric tolerance capabilities of additive manufacturing systems for polymers. Addit Manuf 2020;32:101103. https://doi.org/10.1016/J.ADDMA.2020.101103.
[37] Mac G, Pearce H, Karri R, Gupta N. Uncertainty quantification in dimensions dataset of additive manufactured NIST standard test artifact. Data Brief 2021;38:107286. https://doi.org/10.1016/J.DIB.2021.107286.
[38] Stratasys Ltd. Stratasys J826 prime and J850 prime. Tech. rep. 2021.
[39] Wei X, Bhardwaj A, Shih CC, Zeng L, Tai B, Pei Z. Experimental investigation of Stratasys J750 PolyJet printer: effects of orientation and layer thickness on mechanical properties. In: ASME 2019 14th international manufacturing science and engineering conference; 2019.
[40] Su FY, Sabet FA, Tang K, Garner S, Pang S, Tolley MT, et al. Scale and size effects on the mechanical properties of bioinspired 3D printed two-phase composites. J Mater Res Technol 2020;9(6):14944–60. https://doi.org/10.1016/J.JMRT.2020.10.052.
[41] Singleton L, Cheer J, Daley S. A locally resonant elastic metamaterial utilising multi-material additive manufacturing. In: Proceedings of ISMA2022; 2022.
[42] Qureshi A, Li B, Tan KT. Numerical investigation of band gaps in 3D printed cantilever-in-mass metamaterials. Sci Rep 2016;6(1):1–10. https://doi.org/10.1038/srep28314.
[43] Karami MA, Inman DJ. Analytical modeling and experimental verification of the vibrations of the zigzag microstructure for energy harvesting. J Vib Acoust 2011;133(1). https://doi.org/10.1115/1.4002783.